Simulative Determination of Effective Mechanical Properties for Digitally Generated Foam Geometries

Martin Reder, *Jana Holland-Cunz,* *Paula Lorson, Anastasia August, and Britta Nestler*

Metal foams constitute a promising and emerging material class in the context of lightweight construction. There exists a variety of different foam topologies, on which resulting mechanical properties depend. To maximize the potential of foams in material use under mechanical load, the present work addresses the question how different geometrical parameters influence the material behaviour. Therefore, an algorithm for digital generation and design of open pore foam structures is presented, that allows to regulate the geometry precisely. A method for retrieving effective mechanical properties from numerical simulations of compression tests in the elastic regime is introduced. Additionally, the representativeness of foam volumes considered for simulations is investigated. This yields a fully digital workflow, which enables the investigation of geometry influence on mechanical properties. This approach is used to conduct simulation studies on generated foam structures with a systematic variation of geometrical parameters. Herein, a range of effective Young's moduli varying by up to a factor of 1.3 for different foam structures at the same porosity is found. This shows a significant impact of the foam geometry on the elastic properties of metal foams. The presented methodology yields insights, which can guide design and optimization of materials for specific applications.

1. Introduction

Metal foams are of great interest in many engineering applications since they exhibit some beneficial material properties. This involves particular features such as a large surface-to-volume ratio, as well as relatively high stiffness at low weight. The structure of metallic foams can either have close or open pores, which exhibit different pore arrangements and size distributions. Metal foams show good thermal conductivity due to their large surface area, making them attractive for energy systems.[1] Open pore foams also enable a flow through, which is made use of, for example, in the field of heat exchangers.[2] Besides thermal applications, metal foams also exhibit promising properties with respect to lightweight construction due to their high strength-to-weight ratio.[3] Another aspect is the high energy absorption capability,[4] which is of interest, for example, in crash application.[5]

Besides the metal used for the foams, their structure geometry has an impact on the resulting mechanical properties of the foam.[6] Thereby, not only the volume fraction of the metal plays a role, but the mechanical properties also strongly depend on the foam topology.[7–9] The class of foams contains a large variety of complex structures with a wide range of geometrical parameters, that can vary, such as the ligament cross-section geometry, the ligament alignment, as well as the distributions of ligament thickness and pore size.[9] This spans a large parameter room, which can be subjected to an optimization in order to have a favorable combination of mechanical properties and low mass density. Additive manufacturing such as selective laser melting nowadays allows 3D printing for a wide range of materials, including metals cf., for example.[10,11] This offers the flexibility to realize arbitrarily complex structures. However, the relatively high cost of these processes makes it desirable, to identify promising geometries a priori.

Digital methods for generation and investigation of foam structures offer the possibility for a design space exploration as well as the systematical investigation of the influence, a specific geometrical parameter has on the effective material behavior. The present work thereby focuses on mechanical properties by examining the influence of foam morphology on the effective stiffness. Therefore, based on preceding work, an advanced method for digital generation of foam structures with distinct

M. Reder, B. Nestler
Institute for Applied Materials - MMS
Karlsruhe Institute of Technology (KIT)
Straße am Forum 7, 76131 Karlsruhe, Germany
E-mail: martin_dominik.reder@h-ka.de

M. Reder, J. Holland-Cunz, A. August, B. Nestler
Institute of Digital Materials Science (IDM)
Karlsruhe University of Applied Sciences
Moltkestrasse 30, 76133 Karlsruhe, Germany
E-mail: jana.holland-cunz@kit.edu

J. Holland-Cunz, P. Lorson, A. August, B. Nestler
Institute of Nanotechnology (INT)
Karlsruhe Institute of Technology (KIT)
Hermann-von-Helmholtz-Platz 1, 76344 Eggenstein-Leopoldshafen, Germany

geometrical characteristics is introduced and an approach for simulation and homogenization of the elastic properties is presented. This yields a fully digital workflow, which enables the creation and investigation of different foam structures regarding their elastic properties. It is applied for simulation studies addressing the variation of specific geometrical features of foam structures. Additionally, the workflow offers potential for automatization, for example within an optimization algorithm employing heuristic search, which is part of future work.

Regarding the structure generation, we present an advanced algorithm based on a compact but random sphere packing in our previous work.[12] The set of middle points of these spheres is used for a Voronoi decomposition, with subsequent design of the shape of the ligaments. This algorithm was preceded by many more rudimentary models for the generation of open-pored foam structures. Gibson and Ashby (GA)[13] have a simple cubic pore model for calculation of relative density. The ligaments have a square cal cross section with constant side length. The pore volume is the same in all pores, and the ligaments are at right angles to each other. In his pore model, Zhang[14] assumes the cell geometry of a tetrakaidecahedron. A tetrakaidecahedron has 14 faces, of which 6 faces are quadrilaterals and the remaining 8 faces have 6 corners. Like GA, Zhang also used a square cross section for the bridges. When these polyhedron cells are lined up, a very regular structure is created. A generation of foams with different pore sizes is not possible because tetrakaidecahedrons of different sizes cannot be combined to form a seamless structure. Menges and Knipschild[15] used a pore model with cells in the form of a pentagonal dodecahedron. However, this structure is not space filling, so it is not possible to line up the polyhedra without gaps. The ligaments have a triangular cross section, but the ligament thickness is also constant. Three ligaments meet at each node. This gives the nodes the shape of a tetrahedron, that is, a pyramid base has an equilateral triangle and whose three sides are also equilateral triangles congruent to the base. There are a few other models[16–18] that all have certain things in common. They also follow similar approaches to the geometric models already described. None of these variants go into more detail about the ligament shape or the distribution of the pores. Redenbach[19] however made remarkable progress. In her work, she presents a model that does far more justice to the properties of real foams like the local heterogeneity of pores and ridges relating to the shape and the size, as well as the presence of closed walls. In recent works, structure generation approaches based on Voronoi tessellation have been applied to model different physical properties of closed and open cell foams.[20,21] These approaches yield foam models representing the structural properties of real foams. The foam microstructure is modeled with regard to the randomness of pore sizes, and thus, the characteristics of real foams are well captured.[22] In the present work, we introduce an improved algorithm for digital generation of foam structures. This enables the systematic regulation of the foam topology and the precise control of geometrical parameters. To capture the stochastic nature and morphological properties of real open pore foams, a set of foams with various morphological parameters is generated and tested in simulated quasistatic compression experiments.

Numerical simulations within the elastic regime enable to access both the effective stiffness and yield strength of a structure.[23] Since the generated foam structures exhibit a very complex topology, simulating their response to mechanical load poses a challenging task with regard to numerical discretization. Previous research work used finite-element structure mechanics simulations to investigate the mechanical properties of specific foam structures.[7,23,24]

Since we aim at considering 3D simulations on a variety of different geometries, we used a phase-field method for geometry parameterization of the foam structures. Due to the diffuse interface modeling, the approach enables a numerical treatment on arbitrary grids.[25] In particular, any topology can be considered using a Cartesian grid and thus complicated mesh generation is avoided. This brings the flexibility to simulate various structures without any specific numerical treatment and therefore also offers the potential for automatization. We conduct structure simulations of the generated foam structures in an elastic regime using a phase-field-based solver for structure mechanics within the PACE3D framework.[26]

A method for homogenization of the full-field simulation results is introduced, which assumes isotropic effective behavior for structures that are generated in a statistically isotropic way. This method is based on a least squares fit for a single loading scenario. In contrast to simple homogenization, that only considers the main loading direction as in ref. [7], the quality of the least squares fit yields an indicator in order to judge the isotropy assumption and the representativeness of the considered domain. Additionally, this approach still avoids simulations of different loading scenarios for each particular structure, as it would be required in the general case cf., for example.[27] Thus, it saves computational cost, which is an important factor if a wide parameter space with respect to the geometry should be covered. The approach for determining the effective stiffness is validated via application of the present homogenization scheme on simulation results. Additionally, an investigation of the representative domain size is done, in order to access information about the volume, above which a foam structure can be considered as isotropic. This is a key aspect for numerical simulations to save as much computational cost as possible by not choosing overly big volumes, while still obtaining representative and thus reliable results.

The presented framework is applied to conduct parameter studies of different foam geometries. Therefore, foam structures with varying morphologies and degrees of order in pore size are digitally generated. Structure mechanical simulations in the small deformation regime with elastic material behavior are conducted on the created foam structures. With the results of these simulations, we investigate the geometry influence on the effective stiffness. It is shown that the geometry of the foam structure affects the resulting effective properties significantly. This even holds for structures, which exhibit similar volume fractions of metal and thus the same weight. For example, we observe a range of effective Young's moduli varying by approximately a factor 1.3 for different foam structures at the same porosity. It is found that at constant porosity, a lower pore size with thinner ligaments is favorable with regard to the stiffness of the foam structure. Additionally, an increased stiffness for structures exhibiting a higher degree of order is observed. In particular, structures generated with a centroidal pore distribution showed the largest effective Young's modulus in our studies.

ADVANCED
SCIENCE NEWS

www.advancedsciencenews.com

ADVANCED
ENGINEERING
MATERIALS

www.aem-journal.com

2. Algorithm for the Generation of Foam Structures

This section describes the construction of digital models of porous structures used for the numerical simulation of compression tests performed in the scope of this article. To digitally generate open pore foam structures with a large morphological variety, algorithmic generation routines were used, with the aim to divide space into a cellular structure. These are implemented as part of the software package PACE3D.[26] The generation routines comprise a wide variability in structural features, such as various cell size distributions or ligament shapes. The resulting generated structures mimic morphological and topological characteristics of real foam structures.

The general routine to generate a single structure is based on arranging points in 3D space according to a spatial Voronoi tessellation. The routine can be divided into the following four steps. 1) Generation of a set of generator points in the domain. 2) Obtainment of Voronoi tessellation: Division of the domain into subdomains (polyhedral cells) formed by Voronoi diagram. A Voronoi diagram consists of the set of points in the domain which are equidistant to at least two nearest generator points. 3) Identification of cell edges. 4) Creation of ligaments along the edges.

The steps 2–4 of the foam generation are visualized in **Figure 1**. Applying this routine results in the separation of the domain into two subdomains; one formed by interconnected ligaments and the other one filled by pore space.

The number of generator points corresponds to the number of cells the structure is divided into, which determines the mean volume of a cell and thus, the resulting pore size of the structure. To take into account a differing dispersion in the cell diameters of foams, we use basically two different approaches with differing features for the cell distribution setting (step 1 and 2). The first routine creates a spatially random distribution of generator points. This statistic distribution leads to a generic Voronoi tessellation of the domain and to the formation of cells with arbitrary cell volume. The second routine aims to generate foam structures with predefined cell size distributions. To obtain the set of generator points which allows for the subsequent

tessellation, we make use of an advanced algorithm as proposed in our previous work.[12] This algorithm is based on a compact but random sphere packing. Upon selection of a cell diameter distribution, a dense packing of spheres with the predefined diameter distribution is generated within the domain. The Voronoi tessellation uses the spheres' centers as generator points.

To further develop any kind of cell structure obtained by the described routine, an algorithm creating centroidal tessellations was applied. The method applied is Lloyd's algorithm.[28] For a generated cell structure, the generator point of each cell is iteratively reset and moved toward the barycenter of each cell. Starting point is an existing cell structure obtained by Voronoi tessellation of a domain. One loop of the iterative process can be summarized in the following steps. 1) Calculation of the barycenter of each cell. 2) Moving of the generator points toward the barycenter. 3) Recalculation of the domain tessellation.

In this work, the described algorithms were applied to generate structures of open pore foams with circular and triangular ligament profile. Cellular structures can be characterized, for example, by their porosity P or the volume fraction C_s of solid material. They are defined as

$$c_s = V_f/V_d \tag{1}$$

$$P = (V_d - V_f)/V_d = 1 - c_s \tag{2}$$

with V_d being the total volume of the domain and V_t the volume of the foam structure. Arbitrary porosity values can be achieved with the present structure generation method. The generated structures investigated in this work exhibit porosities in a range of 74–83%. The effective mass density $\rho = \rho_s c_s$ of a foam material is determined by the density ρ_s of the metal in use as well as the solid volume fraction c_s (or porosity P). Thus, comparing properties of foams at same porosity reveals exclusively the influence of the structure geometry while maintaining the weight. Porosity, ligament thickness and pore size of an open pore foam constitute a set of geometrical parameters, where only two are independent. To achieve a specific target porosity, there are two possible iterative approaches. The first is performed alongside a given pore size distribution and is based on iterative
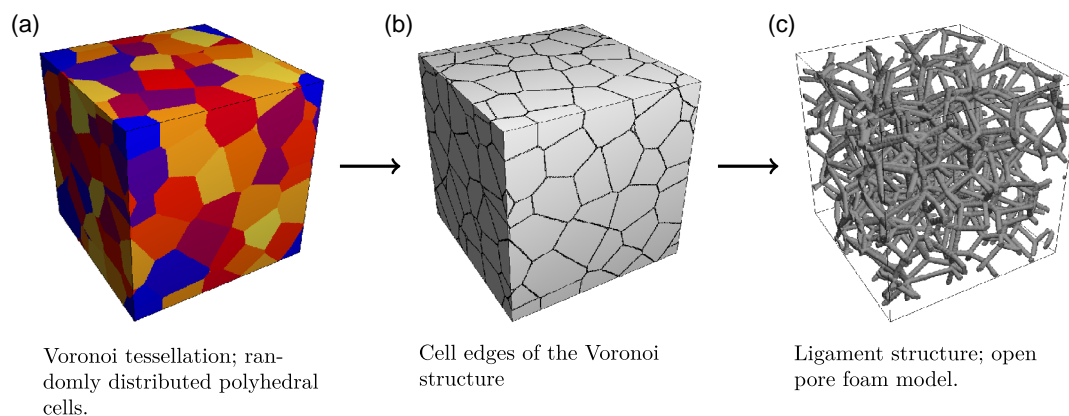

(a) Voronoi tessellation; randomly distributed polyhedral cells.

(b) Cell edges of the Voronoi structure

(c) Ligament structure; open pore foam model.

Figure 1. Schematic graphic of the algorithmic generation procedure for open pore foam structures: a) randomly distributed Voronoi cells obtained by generator points, b) cell edges and vertices, and c) generation of ligaments along the cell edges of (b).

thickening or thinning of ligaments until the target porosity is reached. Alternatively, the ligament thickness can be kept constant, and the pore size is iteratively varied to obtain the target porosity. Three types of foam structures with different underlying random distribution of cells are generated and investigated in the present work. To this end, a set of 54 foam models with generic as well as predefined cell size distributions are generated. For the structures with predefined cell diameter, a normal distribution is used to generate the sphere packing. All models are created on a cubic domain, which is discretized on a Cartesian grid consisting of $400 \times 400 \times 400$ grid cells. Examples of three generated structures with different pore size distributions at constant solid volume fraction C_s are depicted in **Figure 2**.

3. Simulative Determination and Homogenization of Mechanical Properties

3.1. Solution Method for the Mechanical Problem

The mechanical problem is solved using the phase-field-based multiphysics code PACE3D.[26] The stationary momentum balance for small deformations

$$\operatorname{div} \boldsymbol{\sigma} = 0 \tag{3}$$

is considered. Herein $\boldsymbol{\sigma}$ denotes the Cauchy stress tensor. The geometry is parametrized using the phase-field method. Therefore, order parameters ϕ^α for each phase α are introduced, which are field variables representing the local volume fraction of phase α. The transition between two phases is not represented by a jump, but by a thin transition region, where the order parameters exhibit a steep but smooth transition from zero to unity. The stress tensor is calculated according to Khachaturian[29] by means of a linearly interpolated stiffness

$$\mathcal{C} = \sum_{\alpha=1}^{N} \phi^\alpha \mathcal{C}^\alpha \tag{4}$$

where $\mathcal{C}^\alpha$ are the constant phase inherent stiffness tensors. In our case, a two-phase problem is on hand, where the phase representing the pores has a vanishing stiffness, which results in a linear degradation of the metal's stiffness with its phase variable. With the interpolated stiffness, the constitutive law reads

$$\boldsymbol{\sigma} = \mathcal{C}[\boldsymbol{\varepsilon}], \qquad \boldsymbol{\varepsilon} = \frac{1}{2}\left(\operatorname{grad} \mathbf{u} + \operatorname{grad}^\top \mathbf{u}\right) \tag{5}$$

where the infinitesimal strain tensor $\boldsymbol{\varepsilon}$ is the symmetric part of the displacement gradient and the brackets $[\cdot]$ indicate the linear mapping of second-order tensors by a fourth-order tensor. The solution variable is the displacement field $\mathbf{u}$. The momentum balance is solved on a Cartesian grid using a finite-element discretization with linear shape functions and a conjugated gradient method for the solution of the resulting linear system for the node displacements.

3.2. Homogenization Method for Retrieving the Effective Stiffness

The article aims to determine effective elastic properties of metal foams via numerical simulations. Therefore, a homogenization method is required to obtain the effective stiffness from the solution fields' yield by the simulations. In order to do so, we define the volume averaged values of the Cauchy stress tensor σ and the infinitesimal strain tensor ε over the computational domain Ω by means of

$$\overline{\boldsymbol{\sigma}} := \langle \boldsymbol{\sigma} \rangle = \frac{1}{\Omega} \int_\Omega \boldsymbol{\sigma} \, dV \tag{6a}$$

$$\overline{\boldsymbol{\varepsilon}} := \langle \boldsymbol{\varepsilon} \rangle = \frac{1}{\Omega} \int_\Omega \boldsymbol{\varepsilon} \, dV \tag{6b}$$

where $\langle \cdot \rangle$ indicates the volume average. If the domain Ω is a representative volume of the considered metal foam, those averages are proper representations of the effective stress and strain, respectively. Note that both the stress and strain field are obtained by simulations and the respective averages can be calculated from those via numerical integration. In this article, we make the assumption that the Hill–Mandel[30] condition holds. This requires the energy equivalence of the effective stress and strain to the integral energy of the local fields and thus
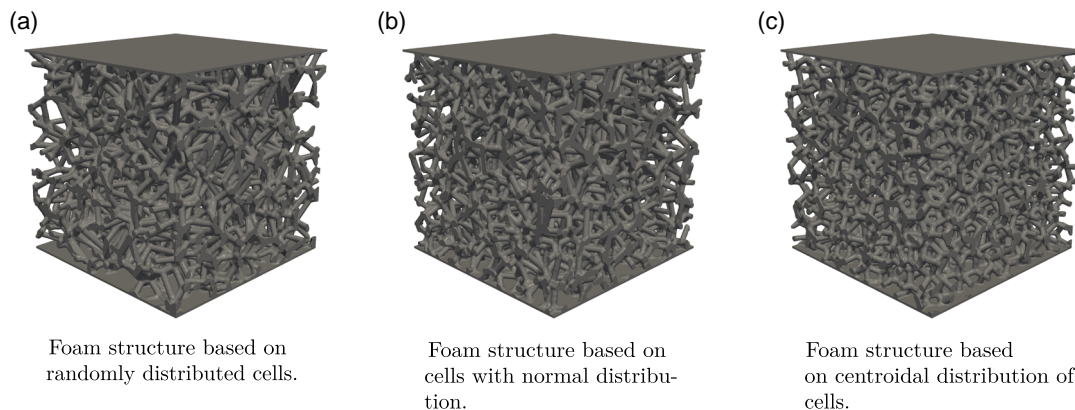

(a) Foam structure based on randomly distributed cells.

(b) Foam structure based on cells with normal distribution.

(c) Foam structure based on centroidal distribution of cells.

Figure 2. Three example foam structures with equal solid volume fraction $c_s = 0.2$, and varying geometries defined by corresponding geometrical parameters of pore size distribution: a) generic distribution, b) normal distribution, c) centroidal distribution.

ADVANCED
SCIENCE NEWS

www.advancedsciencenews.com

ADVANCED
ENGINEERING
MATERIALS

www.aem-journal.com

$$\langle \boldsymbol{\sigma} \cdot \boldsymbol{\varepsilon} \rangle = \overline{\boldsymbol{\sigma}} \cdot \overline{\boldsymbol{\varepsilon}} \tag{7}$$

which implies that the inner power of stress and strain fluctuations $\langle (\boldsymbol{\sigma} - \overline{\boldsymbol{\sigma}}) \cdot (\boldsymbol{\varepsilon} - \overline{\boldsymbol{\varepsilon}}) \rangle$ vanishes. This condition is met for different choices of boundary conditions cf., for example, Saeb et al.[31]. The constant stress boundary conditions used in this work are amongst these. With this, the homogenization problem can be stated such, that an effective stiffness $\overline{\mathcal{C}}$ is to be found, which maps the effective strain onto the effective stress via

$$\overline{\boldsymbol{\sigma}} = \overline{\mathcal{C}}[\overline{\boldsymbol{\varepsilon}}] \tag{8}$$

This can be seen as a search for the elastic parameters of a homogeneous material, which would have the same material response as the considered composite by means of the macroscopic average strain.

The stiffness tensor exhibits the left and right subsymmetry. Additionally, it is main symmetric since we consider hyperelasticity. Thus, in general, there are 21 independent elastic parameters left that need to be determined. Since we consider foams, which are generated with a statistically isotropic method, it is convenient to also assume the resulting effective properties to be isotropic. This of course only holds for a representative volume, which will be investigated in the next section. The isotropy assumption reduces the unknown parameters to two and thus, one load scenario is sufficient to determine those. The isotropic stiffness tensor is

$$\mathcal{C} = \lambda \mathbf{1} \otimes \mathbf{1} + 2\mu \mathcal{I}^{\mathrm{S}} \tag{9}$$

where λ and μ are the Lamé constants, $\mathbf{1}$ the second-order unit tensor and

$$\mathcal{I}^{\mathrm{S}} = \frac{1}{2}[(\mathbf{1}\square\mathbf{1}) + (\mathbf{1}\square\mathbf{1})^{\mathsf{T}_{\mathsf{R}}}] \tag{10}$$

the fourth-order unit tensor with left and right subsymmetry. Herein, the superscript T_{R} indicates the transposition of the right index pair of a fourth-order tensor. The box product $\square$ is defined such, that $(A\square B)[C] = ABC$ holds and thus

$$(\mathbf{1}\square\mathbf{1})_{ijkl} = \delta_{ik}\delta_{lj} \tag{11}$$

is obtained in index notation, where δ_{ij} is the *Kronecker symbol*. The tensorial Equation (7) in this case yields

$$\overline{\boldsymbol{\sigma}} = \overline{\lambda}\mathrm{tr}(\overline{\boldsymbol{\varepsilon}})\mathbf{1} + 2\overline{\mu}\,\overline{\boldsymbol{\varepsilon}} \tag{12}$$

In order to solve this equation, we use a *least-squares method* (LSQ). If the effective material behavior is exactly isotropic, only two of the six equations are linearly independent. However, it cannot be expected that this is exactly the case, since we consider approximate results yield by numerical simulations. Also, the considered volume is finite, and thus the assumptions made for the homogenization are only approximately met. The cost function for the LSQ reads

$$S(\overline{\lambda}, \overline{\mu}) = \sum_{j=1}^{3} \sum_{i=1}^{j} [-\overline{\sigma}_{ij} + 2\overline{\varepsilon}_{ij}\overline{\mu} + \delta_{ij}\mathrm{tr}(\overline{\boldsymbol{\varepsilon}})\overline{\lambda}]^2 \tag{13}$$

Its minimization is done by demanding the necessary condition that the gradients with regard to the parameters vanish. The corresponding partial derivatives are

$$\frac{\partial S}{\partial \overline{\mu}} = \sum_{j=1}^{3} \sum_{i=1}^{j} 4\overline{\varepsilon}_{ij}[-\overline{\sigma}_{ij} + 2\overline{\varepsilon}_{ij}\overline{\mu} + \delta_{ij}\mathrm{tr}(\overline{\boldsymbol{\varepsilon}})\overline{\lambda}] \tag{14}$$

$$\frac{\partial S}{\partial \overline{\lambda}} = \sum_{i=1}^{3} 2\mathrm{tr}(\overline{\boldsymbol{\varepsilon}})[-\overline{\sigma}_{ii} + 2\overline{\varepsilon}_{ii}\overline{\mu} + \mathrm{tr}(\overline{\boldsymbol{\varepsilon}})\overline{\lambda}] \tag{15}$$

From $\partial_{\overline{\mu}}S = 0$ and $\partial_{\overline{\lambda}}S = 0$ the equation system

$$\overline{\mu}\sum_{j=1}^{3}\sum_{i=1}^{j}2\overline{\varepsilon}_{ij}^2 + \overline{\lambda}\mathrm{tr}^2(\overline{\boldsymbol{\varepsilon}}) = \sum_{j=1}^{3}\sum_{i=1}^{j}\overline{\varepsilon}_{ij}\overline{\sigma}_{ij} \tag{16}$$

$$2\overline{\mu}\mathrm{tr}(\overline{\boldsymbol{\varepsilon}}) + 3\overline{\lambda}\mathrm{tr}(\overline{\boldsymbol{\varepsilon}}) = \mathrm{tr}(\overline{\boldsymbol{\sigma}}) \tag{17}$$

is obtained. Its solution with respect to the effective Lamé constants is

$$2\overline{\mu} = \frac{3\sum_{j=1}^{3}\sum_{i=1}^{j}\overline{\varepsilon}_{ij}\overline{\sigma}_{ij} - \mathrm{tr}(\overline{\boldsymbol{\varepsilon}})\mathrm{tr}(\overline{\boldsymbol{\sigma}})}{3\sum_{j=1}^{3}\sum_{i=1}^{j}\overline{\varepsilon}_{ij}^2 - \mathrm{tr}^2(\overline{\boldsymbol{\varepsilon}})} \tag{18}$$

$$\overline{\lambda} = \frac{1}{3}\left[\frac{\mathrm{tr}(\overline{\boldsymbol{\sigma}})}{\mathrm{tr}(\overline{\boldsymbol{\varepsilon}})} - 2\overline{\mu}\right] \tag{19}$$

With this, effective values for the Young's modulus E, the Poisson ratio ν, and the compression modulus K are calculated via

$$\overline{\nu} = \frac{1}{2}\frac{\overline{\lambda}}{\overline{\mu} + \overline{\lambda}}, \qquad \overline{E} = \overline{\mu}\frac{2\overline{\mu} + 3\overline{\lambda}}{\overline{\mu} + \overline{\lambda}}, \qquad \overline{K} = \overline{\lambda} + \frac{2}{3}\overline{\mu} \tag{20}$$

In order to quantify the quality of the least squares fit of Equation (7), we define some error quantities. The component-wise root-mean-square (RMS) deviation is

$$e^{\mathrm{rms}} = \sqrt{\frac{1}{6}\sum_{j=1}^{3}\sum_{i=1}^{j}[-\overline{\sigma}_{ij} + 2\overline{\varepsilon}_{ij}\overline{\mu} + \delta_{ij}\mathrm{tr}(\overline{\boldsymbol{\varepsilon}})\overline{\lambda}]^2} \tag{21}$$

A normalization with the RMS value of the stress tensor

$$\sigma^{\mathrm{rms}} = \sqrt{\frac{1}{6}\sum_{j=1}^{3}\sum_{i=1}^{j}\overline{\sigma}_{ij}^2} \tag{22}$$

yields the relative deviation

$$e^{\mathrm{rel}} := \frac{e^{\mathrm{rms}}}{\sigma^{\mathrm{rms}}} \tag{23}$$

This measure is used as an indicator for quality of the solution fit and thus how good the assumption of an isotropic effective stiffness is. A validation of the presented homogenization approach with respect to the Eshelby single-inhomogeneity problem (SIP) can be found in the Appendix A.

3.3. Description of the Simulation Setup

In order to retrieve the effective elastic properties of a metal foam, we conduct simulations, where uniaxial tension is applied on the foam structure. To ensure a comparable loading situation, the foam is placed in between two plates of the same material, which exhibits the Young's modulus E_s. On those plates, constant stress boundary conditions $t = \pm\sigma^{BC}e_y$ are applied, as shown in the schematic **Figure 3**. The averaging domain for the homogenization excludes the plates and only contains the actual foam.

3.4. Investigation of the Influence of the Domain Size on Isotropy

In this section, the presented approach for simulation and homogenization is applied to an open pore foam structure. The influence of the domain size on the isotropy of the effective stiffness is investigated in order to validate this assumption. Therefore, a Voronoi foam with circular ligaments and a normal distribution for the cells is considered, which is generated using the algorithm described in Section 2. This yields a statistical foam, where the pore-size s and the ligament thickness d_s by means of the ligament diameter obey a Gaussian distribution, whose expectation value and standard deviation can be specified. The pore size is defined as the maximum diameter of a sphere placed in a pore's barycenter that does not lead to overlap with the sphere of a neighboring pore, as depicted in Figure 3.

We consider four different domain sizes, where the statistical properties of the respective foam geometry are similar by means of the expectation value $EW(s)$ of the pore size, its standard deviation σ_s, and the mean ligament thickness d_s. The edge Length L of the considered domain varies over the four simulations from

four times to ten times the mean pore size and therefore, the resulting number of pores within the domain goes from 40 to 560 (for details, see **Table 1**). The length of the smallest domain L_I is used as characteristic length, with respect to which all other length scales are given. Simulations of a compression test in each coordinate direction are performed for every structure, respectively, setup. Exemplarily, the results of the three simulations related to setup III are shown in **Figure 4**. The resolution for setup I is $125 \times 125 \times 125$ elements and the element numbers are increased corresponding to the domain size. For the evaluation, we consider the tuple $\mathbb{E} = \{\overline{E}_1, \overline{E}_2, \overline{E}_3\}$ of effective Young's moduli yield by the three compression tests for each structure. We define the average of this tuple via

$$\overline{E}^m := \frac{1}{3}\sum_{i=1}^{3}\overline{E}_i \tag{24}$$

and the deviation

$$A := \frac{\max(\mathbb{E}) - \min(\mathbb{E})}{\overline{E}^m} \tag{25}$$

which yields a relative measure for the difference in effective Young's moduli for the different load directions.

Figure 5 shows the tuple mean value $\overline{E}^m$ of the effective Young's moduli, which is normalized by the Voigt bound $\overline{E}^V$ as well as the deviations A and e^{rel}. The Voigt bound[32] is the upper limit for the stiffness and corresponds to the arithmetic mean of the phase-wise stiffness tensors with the corresponding volume fraction.[33] Thus, in the present case it is given by

$$\overline{E}^V = c_s E_s \tag{26}$$

regarding the Young's modulus, where c_s is the total volume fraction of the foam material and E_s its Young's modulus. The error bars in the plot represent the maximum deviation of the corresponding value within the simulation tuple of the three loading directions. For the two small domain sizes, the effective Young's modulus is approximated poorly. The deviation between the three directions is large, which indicates that the effective stiffness is not isotropic for those cases. Additionally, the effective Young's modulus is underestimated. Compared to that, the two larger domains only show small directional variation and
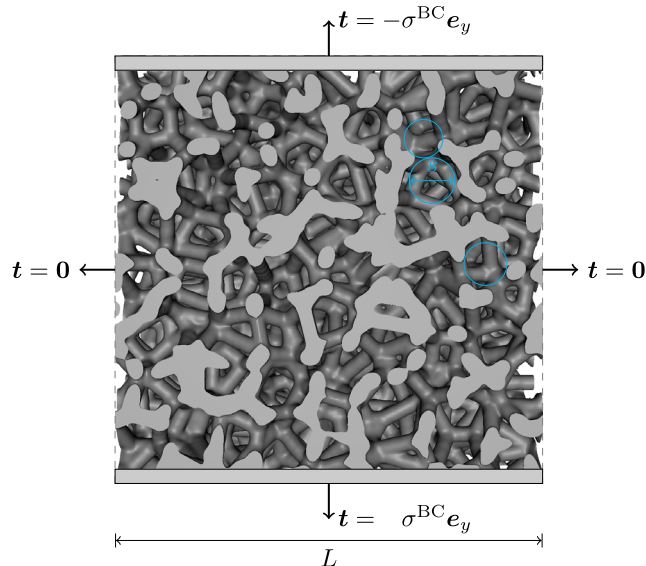

Figure 3. Schematic of a slice in y-direction with boundary conditions, where $t = \sigma n$ is the stress vector. The pore size is defined by the diameter s of the sphere placed in the pores center that does not overlap with the one of a neighboring pore. This is visualized by blue circles.

Table 1. Geometrical parameters of the considered foam. Length scales are given relative to the smallest domain length L_I used as characteristic value. Tabulated quantities are the number of pores, domain length L/L_I, pore size distribution ($L/EW(s)$, L_I/σ_s), ligament thickness L_I/d_s, and resulting volume fraction c_s. The ligament thickness and statistical distribution of pore-size are constant in all setups, while the length of the domain L (and thus the domain size) is varied.

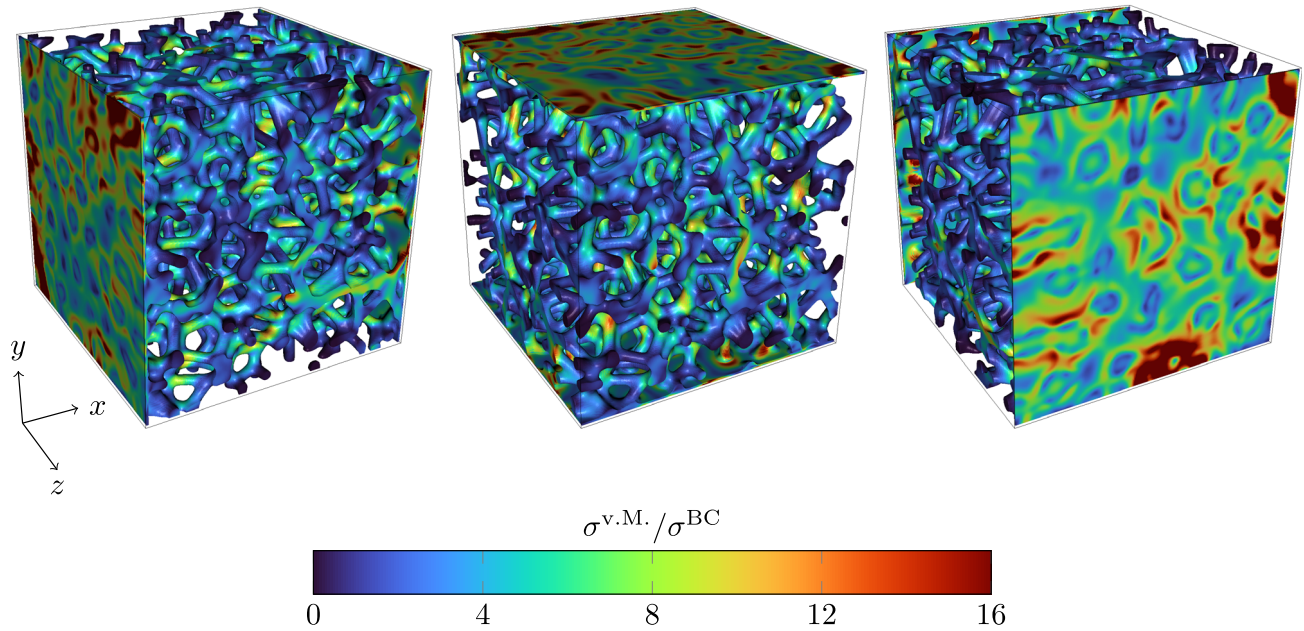| setup	pores	L/L_I	$L/EW(s)$	L_I/σ_s	L_I/d_s	c_s
I	40	1	4	40	12.5	0.31
II	109	$\frac{3}{2}$	6	40	12.5	0.32
III	279	2	8	40	12.5	0.33
IV	560	$\frac{5}{2}$	10	40	12.5	0.31

Figure 4. Compression tests of an open pore foam in the three spatial directions displayed for the setup III (see Table 1). Von Mises stress $\sigma^{\mathrm{v.M.}}$ normalized with the boundary stress σ^{BC} is applied at the phase-field isosurface with a value of $\phi^s = 0.2$.
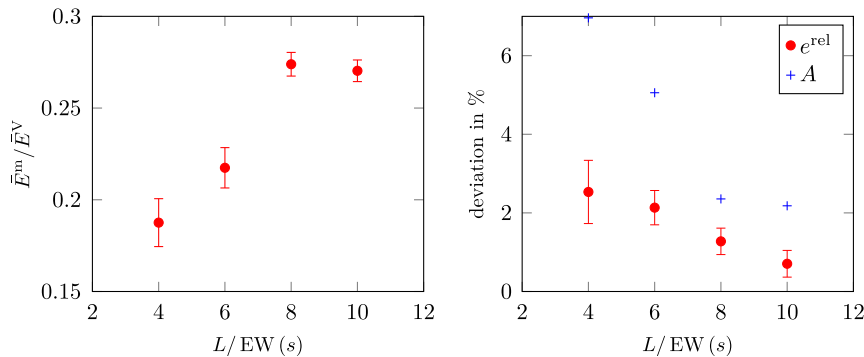

Figure 5. Effective properties depending on the considered domain size. The mean values of pore size and ligament thickness remain unchanged. Left: Effective Young's modulus by means of Equation (23) normalized with the corresponding Voigt bound $\overline{E}^V = c_s E_s$. Right: relative error e^{rel} according to Equation (22) and the deviation$A$ according to (22). The error bars mark the maximum deviation with respect to the tuple of the three loading directions $\max_{i\in\{1,2,3\}}|\overline{E}^m - \overline{E}_i|$.

they both yield similar values for the effective Young's modulus, which is in the region around 27% of the Voigt bound. For the present volume fraction $c_s \approx 0.32$, this corresponds to $\overline{E}/E_s \approx 0.086$ and thus 8.6% of the full material's stiffness. In addition to the first-order Voigt bound, the second-order Hashin–Shtrinkman (HS) bounds[34] are applicable in this case, since quasi-isotropic effective behavior is considered. The upper HS bound is more restrictive than the Voigt bound and introduces a dependency of the Young's modulus limit $\overline{E}^{HS}$ on the solid materials' Poisson ratio, which is not the case for the Voigt bound, if one phase exhibits zero stiffness. For the present structure of a material with a Poisson ratio of 0.35, $\overline{E}^V = 0.32E_s$ and $\overline{E}^{HS} = 0.19E_s$ are obtained, and thus, the HS bound is

significantly more restrictive. The foam structure reaches $\overline{E}/\overline{E}^{HS} = 45.3\%$ with regard to the HS bound.

Based on a modeling of cubic unit cell foams, GA[13] derived the correlation

$$\frac{\overline{E}}{\overline{E}^V} = k c_s \tag{27}$$

for the ratio of the effective Young's modulus $\overline{E}$ with the Voigt bound $\overline{E}^V$ according to Equation (A1). Herein, c_s denotes the volume fraction of foam material and k the structural factor. This factor was proposed to be near unity for open pore foams. However, the choice of $k \approx 1$ is based on a unit cell model, which

**ADVANCED
SCIENCE NEWS**

www.advancedsciencenews.com

**ADVANCED
ENGINEERING
MATERIALS**

www.aem-journal.com

assumes a regular structure and the ligaments as beams with constant cross section[9] and thus, does not account for geometrical irregularities, which have a large impact on the structural factor, cf., for example.[6,7] A fit to k for results of setup III and IV yields a value $k \approx 0.88$, which is significant below unity. However, larger structural factors above unity can be realized also for normal pore distributions by varying the pore size and ligament thickness, as shown and discussed in Section 4.

From the right graph in Figure 5, it can be seen that for setup III and IV, and thus $L/\text{EW}(s) \geq 8$, the influence of the loading direction is very small, such that isotropic effective behavior is a fair assumption in those cases. This implies, that one simulation in a single loading direction is sufficient to retrieve a proper approximation of the effective stiffness and therefore the computational time for consideration of different loading scenarios can be saved. The error measure e^{rel} for each loading direction shows the same trend as the actual deviation A. However, for the small domain sizes, e^{rel} shows larger variations. Hence, it might be an underestimation. Still a large value of the least squares error as $e^{\text{rel}} \gtrsim 2\%$ indicates a nonrepresentative and thus insufficient domain size. Therefore, this error measure still allows judging the quality of the simulation and homogenization results. As a result of this investigation, it can be stated that the size of the computational domain should be at least eight times the mean pore size in order to retrieve an isotropic effective behavior. This corresponds to a minimum number of ≈ 280 pores inside the domain, which is required for it to be a representative volume. This is ensured in the following parametric study.

4. Parametric Studies for Varying Foam Geometries

The primary objective of this study is to investigate how different geometrical parameters influence the mechanical material behavior of a given foam structure. To achieve this goal, a series of numerical experiments are conducted. Variation of the geometrical parameters and measurement of the resulting changes in material properties serve as key points for the simulative investigation. Therefore, digital compression tests in the elastic regime are used using the numerical method presented in this work. In all simulations, foam volumes with at least 500 pores and thus, a domain length approximately above 9 to 10 times the mean pore diameter are considered ensuring appropriate representativeness of the domain according to the results of the previous section. Subsequently, a characteristic length is used to normalize all other occurring length scales. It also defines a unit volume, which serves as reference. Since linear elasticity is considered, the following results are independent of the length scale. The simulation results yield various information regarding the mechanical properties arising for a foam structure. This includes the effective stiffness by means of elastic constants like Young's modulus and Poisson ratio. Additionally, field information is obtained, for example, for the von Mises stress $\sigma^{\text{v.M.}}$, whose value indicates, where local plastification will start, if the yield strength is reached. Thus, the results of these experiments can provide additional insights into the complex

relationship between geometry and material behavior, which have important implications for the design and optimization of materials and structures. For example, the results can reveal points with local high stress amplification by means of $\sigma^{\text{v.M.}}/\sigma^{\text{BC}}$, as shown in Figure 4. This information could be used to actively optimize structures. However, such analysis is out of scope of this article. Subsequently, we restrict the evaluation to the effective Young's modulus as an indicator to judge the overall mechanical properties a foam structure exhibits. Thus, the presented homogenization method is well suited to answer the objective of the study at hand.

To analyze the impact of foam geometry on the effective stiffness, a set of 3D foam structures with varying structural properties was generated and examined. At first, different foam geometries are investigated at a constant solid volume fraction of $c_s = 0.2$. Thereby, a total of 18 structures are compared. The structures feature three different types of cell distributions, generic, normal, and centroidal. For the structures examined in this study, the ligament profile takes both circular and triangular shape, with equivalent cross-sectional area. For each type, structures differing in pore density are considered. A discussion on the corresponding length scales is given in Appendix B. The homogenized value of effective stiffness was determined from spatially resolved field data following the presented homogenization approach. Subsequently, the effective Young's modulus is given normalized with the Voigt bound $\overline{E}^V$. This results in a measure for the ratio with respect to the theoretical maximum stiffness at a given volume fraction c_s and thus a reference with comparable material weight. Therefore, this serves as a more meaningful choice compared to a normalization with the pure solid value E_s, which is commonly used in literature. Note, that the relation $\overline{E}^V = c_s E_s$ holds. The results show that the cell structure, the ligament profile, and the pore density of the materials play a crucial role in their behavior. Although the porosity remains at a constant value, the calculated value for the normalized effective Young's modulus varies depending on the structure type and pore density. The results of this study are depicted in **Figure 6**.

The structures with centroidal distribution show the highest effective stiffness in the explored range, whereas structures with normal distribution of cell size yield reduced values, followed by structures with generic distribution which lead to the lowest values. This implies that the degree of order in cell structure enhances effective stiffness. At constant pore size, we find the stiffness of foams with centroidal and generic distribution varies by a factor of around 1.3. For all the structure types investigated, the samples with triangular shaped ligaments are found to have higher effective stiffness than the ones with circular ligaments. The results for the pore density variation show that there is an increasing trend in the normalized effective Young's modulus with larger numbers of pores per unit volume. At constant porosity, this indicates that fine structures with small pores and ligaments maximize the effective stiffness. In addition, it is observed that the variation in cell size distribution has stronger influence compared to changes of the cross-sectional ligament profile. Our finding that more regular foam structures lead to a higher effective stiffness is in good agreement with, for example, Kaoua et al.[35] In their work, they consider foams with quadratic unit
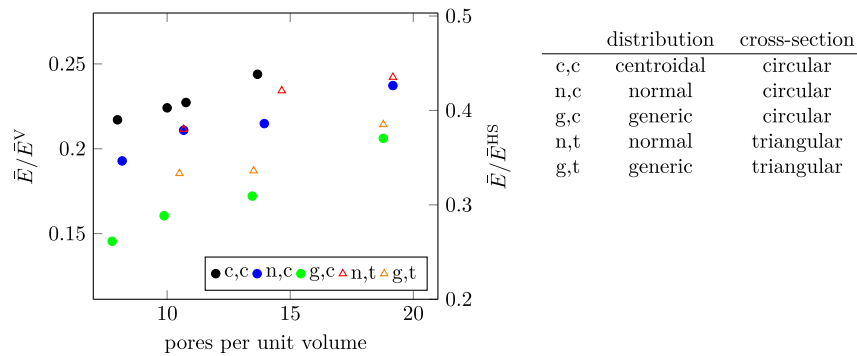
distribution	cross-section
c,c	centroidal	circular
n,c	normal	circular
g,c	generic	circular
n,t	normal	triangular
g,t	generic	triangular

Figure 6. Influence of pore size and ligament thickness at constant solid volume fraction $c_s = 0.2$ ($P = 80\%$). Effective Young's modulus $\overline{E}$ normalized with the Voigt bound $\overline{E}^V = c_s E_s$ over pores per unit volume for different cross-section geometries and pore distributions according to the table on the right. A higher number of pores per unit volume indicates smaller pore size as well as smaller ligament thickness. The right axis shows $\overline{E}$ normalized by the HS bound $\overline{E}^{HS}$. The points with ≈ 10 pores per unit volume of each structure correspond to the respective values of $c_s = 0.2$ in Figure 7.

cells under varying strut alignment and find the stiffness in a range of approximately factor 1.27 between perfectly aligned and irregularly aligned struts.

In a second study, three different types of foam geometries are chosen from the ensemble above. The aim is to investigate the influence of porosity on effective elastic properties of open porous structures. The predicted values of the effective stiffness were analyzed for systematically varied values of porosity. The first type of geometry features a generic cell size distribution, the second a predefined normal distribution of cell sizes, and the third a centroidal distribution. The complete set of geometries evaluated possesses circular ligaments. Due to comparability, a set of 13 structures for each type of geometry is evaluated, where the solid volume fraction varies within a range of $c_s \in [0.17, 0.26]$. Thereby, c_s is regulated over the pore size, while the ligament thickness is held constant. The reason for this choice is, that from the results of the preceding study (cf. Figure 6), we expect higher stiffness if the volume fraction is altered by reducing the pore size instead of increasing the ligament thickness. The results of this study demonstrate a clear correlation between porosity, cell size distribution, and the effective elastic properties of the considered structures. To visualize the relationship between porosity and normalized effective Young's modulus, the data obtained are depicted in the Ashby plot shown in **Figure 7**. Using the effective stiffness yield by these simulations, a fit of the structural factor k is obtained by means of a LSQ-method of the GA correlation (24). The respective fits as well as the suggested factor $k = 1$ from GA[13] are also plotted in Figure 7. The resulting structural factors of the LSQ-fit are given in **Table 2** alongside the root-mean-square (RMS) deviation with respect to the fit. The latter is given both for the absolute deviation and a relative deviation normalized with the values of the fit. The relative RMS deviation is below 4% in all cases. For the normal and generic distribution, the linear fit is less accurate, while the centroidal structures yield a value of 1.7% and thus, good agreement of simulation results and the linear GA correlation. This finding is plausible, since the correlation was derived from regular structures. Hence, a better agreement for structures with a higher degree of order is expected. A more detailed discussion on the influence of the random seed used for the
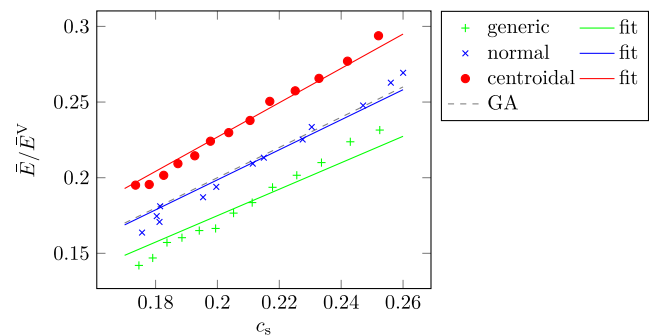

Figure 7. Effective Young's modulus $\overline{E}$ normalized with the Voigt bound $\overline{E}^V = c_s E_s$ over the volume fraction c_s of solid phase. Foams with circular ligament cross section and different distributions are considered, namely, generic, normal, and centroidal, alongside their linear LSQ fit (see Table 2). Additionally, the GA relation with structural factor $k = 1$ is plotted (black). At $c_s = 0.2$, approximately 10 pores per unit volume are considered (see Figure 6).

Table 2. Least squares fit for linear ansatz of $\overline{E}/\overline{E}^V$ with respect to c_s according to Equation (26) (GA) for different foam structures. The structural factor k as well as the absolute and relative RMS deviation of the fit is given.

Structure	k	Absolute RMS	Relative RMS [%]
Generic	0.87450	0.0070043	3.8994
Normal	0.99294	0.0062808	3.0775
centroidal	1.1344	0.0038999	1.6802

Voronoi tessellation can be found in Appendix C. The different foam geometries lead to diverse structural factors varying between 0.87450 and 1.1344. The normal pore size distribution yields a value very similar to unity as the one proposed by GA.[13] However, also structural factors significantly below and above unity can be realized with the generic and centroidal distribution, respectively. Therefore, a significant impact of the structure geometry onto the effective stiffness is observed. Structures with

a higher level of order display greater effective Young's modulus, as observed in our studies. In particular, structures generated with a centroidal pore distribution exhibited the highest values for effective stiffness. Overall, the proposed methodology proved to be well suited to investigate the influence geometrical features of open pore structures have on effective elastic properties at various porosities.

Subsequently, limitations of the presented study are discussed. The question of accuracy with regard to the numerically predicted results arises for different reasons. Discretization errors are introduced both in the simulation results, as well as in the numerical integration to retrieve the effective values. For a single structure, we considered different resolutions and observed small deviations in the result. However, due to computational cost, a convergence study could not be performed for all investigated structures. Additionally, we chose the sample size just as big, as our investigations with regard to representativeness of the domain suggest. Still some errors remain and larger domains would further increase representativeness and thus the accuracy, especially since these investigations were only done for a normal pore size distribution. This may limit the generalizability of our findings. Further studies of both resolution and domain size are desirable to confirm our results quantitatively. To overcome the limitations associated with synthetic structures, it would be valuable to focus on utilizing 3D images of real samples as models for validation to improve the accuracy of conclusions made about their properties. Furthermore, there are several structural variables that could influence the results, but were not controlled for in this study, such as pore size distribution or inhomogeneity in ligament profile. Future research should aim to models which represent these structural properties. Finally, the investigation of further properties should be considered. In this study, we exclusively use the effective Young's modulus as an indicator for the quality of a structure. As already mentioned, a deeper analysis, for example, of the von Mises stress or pressure field would be beneficial, since those could show different trends compared to the effective stiffness.

In summary, the application of the homogenization method was proven to be a versatile tool to retrieve effective elastic properties for open-pore metal foams. The main goal of this research was to understand the impact of various geometric factors on the mechanical performance of a foam structure. GA-type correlations were established in order to link the effective stiffness with the porosity under differing structural parameters. The findings of this work might have the potential to provide further insight into structure–property relationships of porous materials. The results suggest that the investigation can be extended beyond the limitations of this study, opening up new possibilities for understanding the relationship between geometry and material behavior. Therefore, further parameter variations could be considered and besides the Young's modulus additional quantities could be analyzed, for example, the Poisson ratio or statistics regarding the local stress amplification. Furthermore, the application of the presented methodology could be extended to other porous structures to predict their elastic behavior under different loading conditions. These findings may guide the design and optimization of open pored metal foams for specific applications and can be used to develop new porous materials with improved properties.

5. Conclusion and Outlook

The present work addresses the influence of metal foam topology on the effective elastic properties of the foam structure. An improved algorithm for digital generation of foam structures is introduced, which enables the generation of structures with defined geometrical parameters, such as the cell distribution (generic, normal, centroidal), the ligament cross-section geometry (circular, triangular), and the pore size distribution. In order to investigate the mechanical behavior of the generated structures, numerical simulations of compression tests in the elastic regime are used. A homogenization method for isotropic foams based on a least square fit is presented in order to retrieve the effective stiffness. With this approach, only the conduction of one simulation is sufficient to retrieve the effective stiffness of a structure and an error measure is yielded, which allows judging the quality of the homogenization. The influence of the domain size is investigated with regard to the isotropy. It is shown that for the considered open pore foams, a representative volume requires an edge length of the domain, which is at least eight times larger than the mean pore size of the foam. This corresponds to a number of at least ≈ 280 pores inside the domain.

Using the presented approach consisting of digital foam generation as well as simulation and homogenization of the corresponding mechanical properties, parametric studies are conducted considering various different foam geometries. It is found that the structure geometry strongly influences the mechanical properties. The structural factor for fitting the GA correlation varies in a range of 0.87450 and 1.1344, within the parametric study. The structure with centroidal cell distribution shows the most beneficial properties with regard to a high effective stiffness. Additionally, at constant porosity, decreasing the pore size (and the ligament thickness correspondingly) leads to an increase in stiffness.

An extension to the present work could be the application of optimization algorithms, which can yield an automated approach for finding favorable structure geometries with respect to a defined cost function (e.g., the effective stiffness). Therefore, methods of heuristic search could be applied, for example, the particle swarm optimization.[36] Also, the extension of the material model to capture the elastoplastic regime is desirable since it enables the investigation of further important properties, which are not covered with a purely elastic consideration. Both aspects will be addressed in future work.

Appendix A

Validation of the homogenization for the Eshelby single inhomogeneity

We consider the Eshelby SIP[37] consisting of a spherical inhomogeneity within an infinitely large matrix and subjected to Neumann boundary conditions. The stiffness of the matrix material is $\mathcal{C}_{\mathrm{m}}$ and the inclusion's stiffness is $\mathcal{C}_i$. For a two-phase problem with phase-wise constant stiffness, the effective stiffness tensor can generally be obtained via

$$\overline{\mathcal{C}} = \mathcal{C}_{\mathrm{m}} + c_i(\mathcal{C}_i - \mathcal{C}_{\mathrm{m}})\langle \mathcal{A} \rangle_i \qquad (A1)$$

where $\mathcal{A}$ is the strain localization tensor with the property

$$\varepsilon = \mathcal{A}[\overline{\varepsilon}] \tag{A2}$$

In the limit of a dilute defect distribution and thus volume fractions of the inhomogeneity $c_i \ll 1$, the strain localization tensor $\mathcal{A}$ is given via the analytic strain field. Exploiting this, the effective compression modulus $\overline{K}$ and the effective shear modulus $\overline{\mu}$ are

$$\overline{K} = K_m + c_i(K_i - K_m)\frac{4\mu_m + 3K_m}{4\mu_m + 3K_i} \tag{A3a}$$

$$\overline{\mu} = \mu_m + c_i(\mu_i - \mu_m)\frac{5\mu_m(4\mu_m + 3K_m)}{6\mu_i(2\mu_m + K_m) + \mu_m(8\mu_m + 9K_m)} \tag{A3b}$$

The isotropic stiffness tensor is retrieved via

$$\mathcal{C} = 3K\mathcal{P}_1 + 2\mu\mathcal{P}_2 \tag{A4}$$

where the split of stress and strain into a spherical and deviatoric part is exploited. Herein and are the respective projectors.

The SIP is solved numerically using a phase-field method and the stress interpolation scheme of Schneider et al.[38] A finite-element discretization of the momentum balance is used on a Cartesian grid with 150×150 elements. The diffuse interface width corresponds to five times the length of a finite element. We consider a rectangular domain of length L, where the size of the inhomogeneity is varied up to a volume fraction of $c_i \approx 30\%$. At the boundary, we employ a stress boundary condition, such that compression with 0.1 MPa is done (see **Figure 8**). The matrix as well as the inclusion has phase-wise constant properties according to **Table 3**.

Figure 9 shows the effective compression and shear modulus over the volume fraction c_i of the inclusion. Depicted are the homogenized simulation results, the analytic solution, as wel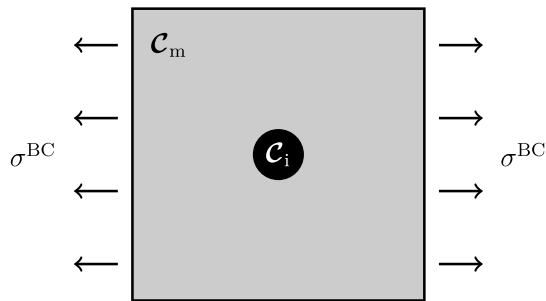l as theoretical bounds. As shown by Hill,[33] the Voigt and Reuss bound are first-order theoretical limits for the stiffness corresponding to an arithmetic and harmonic mean of the stiffness tensor, respectively. In the isotropic case, this corresponds to the respective mean value of shear modulus μ and compression modulus K. Additionally, the second-order Hashin–Shtrinkman (HS) bounds[34] are plotted, which yield more restrictive, and thus accurate, limits compared to the first-order bounds. In the present case, the upper HS bound and the Voigt bound almost coincide, while the lower HS bound is significantly higher compared to the Reuss bound. Note, that the analytic solution is only valid for a dilute defect distribution $c_i \ll 1$ and thus is an appropriate validation up to $c_i \lesssim 7\%$. In that region, we find a agreement between the simulative results and the theory.

For the case with an inhomogeneity with diameter 0.3 L, which corresponds to a volume fraction of $c_i = 0.0225\pi \approx 7.1\%$, **Table 4** summarizes the homogenization results. The deviations between simulation and the analytical solution are within the region of 1% or below. They also lie within the theoretical bounds of first and second order, respectively. The indicator for the deviation to an isotropic effective behavior is $e^{\mathrm{rel}} = 0.13\%$ and thus the tensor equation is very well met.

Appendix B

Discussion of length scales arising in the considered problems

For the foams considered in this manuscript, in general, three length scales occur. These are the (mean) pore size s, the (mean) ligament thickness d_s, and the edge length L of the RVE. If a constant volume fraction $c_s = \mathrm{const}$ should be achieved, this constraint allows only two length scales to be chosen independently. For the study in Figure 5, the additional constraint $d_s/s = \mathrm{const}$ is added. Therefore, only the domain length can be varied, which is done in this study. This means that similar foam structures are considered and, as shown in the study, varying L has no impact as long as the volume is still representative. In contrast, for Figure 6, the constraints $c_s = \mathrm{const}$ and $L = \mathrm{const}$ are considered and thus, a fix domain volume is used. Again, only one of the three length scales can be chosen. If a smaller pore size is considered, meaning a larger amount of pores in the volume, the ligament thickness decreases accordingly in order to obtain the constant solid volume fraction. This yields a different foam with different mechanical properties, as shown in Figure 6. This is the case even though all the foams exhibit the same volume fraction of solid and thus same weight. In **Figure 10**, the correlations between ligament thickness, pore size, and pores per unit volume are depicted for the structures from Figure 6.

Appendix C

Influence of the random seed for generic distributions

The structures with the generic pore size distribution are the most irregular ones investigated in the present article, and thus they show higher deviations with respect to the effective stiffness compared to the normal and especially the centroidal distribution (see Table 2). Therefore, we use different generic distributions to investigate the influence of the randomness of the strongly

Figure 8. Computational setup for the Eshelby SIP.

Table 3. Material properties of the Eshelby SIP.

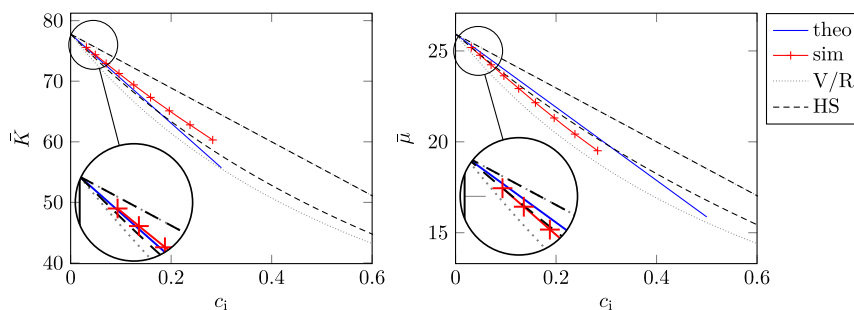| Quantity	Matrix	Inhomogeneity
E in GPa	70	30
ν	0.35	0.35
μ in GPa	25.9	11.$\overline{1}$
λ in GPa	60.5	25.9
K in GPa	77.$\overline{7}$	33.$\overline{3}$

Figure 9. Effective material properties over the volume fraction of the inclusion. Analytic solution for $c_i \ll 1$ (theo) according to Equation (A3a,b), simulation result (sim), and theoretical bounds. These are Voigt[32] and Reuss[39] bound (V/R) as well as the second-order Hashin–Shtrinkman bounds[34] (HS).

Table 4. Comparison of effective properties for the SIP with $c_i \approx 7.1\%$. Simulation result (sim), analytical solution (theo), and the relative deviation between both. Additionally, the theoretical bounds of both first and second order are listed. The absolute values are given in GPa.

Quantity	sim	theo	Deviation	Voigt	Reuss	HS+	HS−
E	65.46	66.08	−0.933%	67.17	63.97	65.69	64.99
μ	24.24	24.50	−1.087%	24.88	23.69	24.36	24.10
λ	56.75	56.25	0.901%	58.05	55.29	55.94	55.34
K	72.91	72.58	0.454%	74.64	71.08	72.18	71.40

Figure 11. Comparison of the influence for different random seeds and the generic pore size distribution. The structural factors for different seeds are $k = 0.84075$, $k = 0.87450$, and $k = 0.83193$, respectively. The corresponding relative RMS deviations of the fit are 5.5828%, 3.8994%, and 4.6619%.

inhomogeneous structures, which is represented by the random seed employed in the structure generation algorithm. Simulations with three different random seeds are performed. Additionally, an ensemble average of the three seeds is considered. The results are shown in **Figure 11** alongside the corresponding GA fit. Seed 3 and even more seed 1 yield some nonmonotonic behavior in c_s and thus quite large deviation of the fit. The ensemble of all three yields $k = 0.85552$, with RMS error of 4.3187%. Seed 2 yields the best fit and a monotonic behavior and is therefore used in Figure 7. The relatively high impact of the random seed limits the high significance of quantitative results for the generic distribution. Still, the tendency of $k \approx 0.85(\pm 0.05)$ is observed. Thus, a significantly lower structural factor than normal and centroidal distribution can still
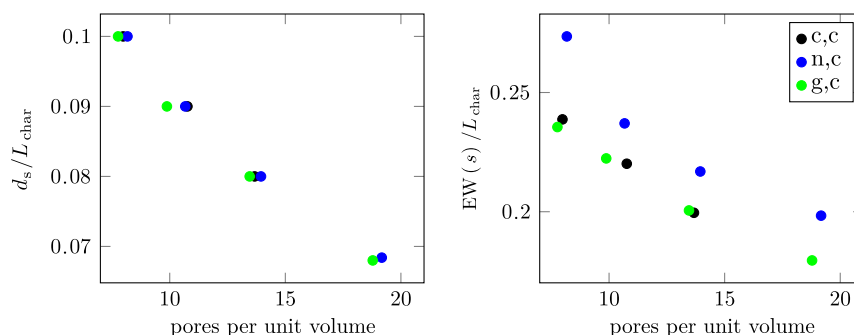
be stated clearly. Note that the normal and centroidal distributions yield higher degree of order in the resulting structure and therefore show less deviation and a way better fit to the GA correlation. This holds in particular for the centroidal distribution. Despite the relatively high deviation of the results for the generic structures, they still support the key point of the present article, which is, that a strong influence of the foam geometry onto the effective stiffness exists.

Figure 10. Correlation between ligament thickness d_s by means of the ligaments mean diameter, mean pore size EW(s), and pores per unit volume at constant solid volume fraction $c_s = 0.2$ with regard to the structures in Figure 6. The length scales are normalized with the characteristic length $L_{char} \approx L/4$ corresponding to the edge length of the unit volume.
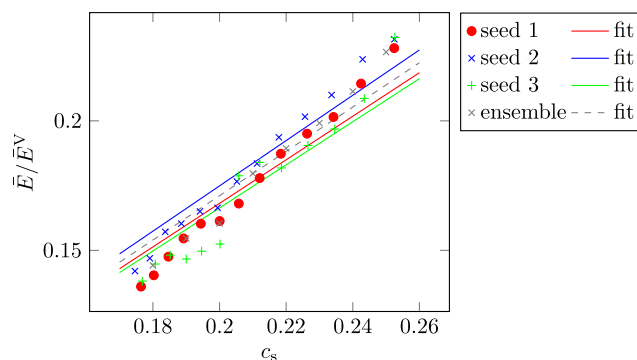
2300340 (12 of 13)

www.advancedsciencenews.com

Conflict of Interest

The authors declare no conflict of interest.

Data Availability Statement

The data that support the findings of this study are available from the corresponding author upon reasonable request.

[1] A. August, A. Reiter, A. Kneer, M. Selzer, B. Nestler, *Heat Mass Transfer Res. J.* **2018**, *7*, 15.

[2] H. Huisseune, S. De Schampheleire, B. Ameel, M. De Paepe, *Int. J. Heat Mass Transfer* **2015**, *89*, 1.

[3] T. Dennis Claar, C.-J. Yu, I. Hall, J. Banhart, J. Baumeister, W. Seeliger, *SAE trans.* **2000**, *98*.

[4] J. Frömert, T. G. Lott, A. M. Matz, N. Jost, *Adv. Eng. Mater.* **2019**, *21*, 1900396.

[5] F. Garca-Moreno, *Materials* **2016**, *9*, 85.

[6] Y. X. Gan, C. Chen, Y. P. Shen, *Int. J. Solids Struct.* **2005**, *42*, 6628.

[7] S. A. Kaoua, S. Boutaleb, D. Dahmoun, M. Azzaz, *Comput. Appl. Math.* **2016**, *35*, 977.

[8] I. Maskery, L. Sturm, A. O. Aremu, A. Panesar, C. B. Williams, C. J. Tuck, R. D. Wildman, I. A. Ashcroft, R. J. M. Hague, *Polymer* **2018**, *152*, 62.

[9] H. X. Zhu, J. R. Hobdell, A. H. Windle, *Acta Mater.* **2000**, *48* 4893.

[10] O. Al-Ketan, R. Rowshan, R. K. Abu Al-Rub, *Addit. Manuf.* **2018**, *19*, 167.

[11] F. Caiazzo, S. L. Campanelli, F. Cardaropoli, N. Contuzzi, V. Sergi, A. D. Ludovico, *Int. J. Adv. Manuf. Technol.* **2017**, *92*, 2121.

[12] A. August, J. Ettrich, M. Rölle, S. Schmid, M. Berghoff, M. Selzer, B. Nestler, *Int. J. Heat Mass Transfer* **2015**, *84*, 800.

[13] L. J. Gibson, M. F. Ashby, *Cellular Solids: Structure and Properties. Cambridge Solid State Science Series*, 2nd ed., Cambridge University Press, Cambridge [u.a.] **1997**.

[14] J. Zhang, *PhD Thesis*, University of Cambridge, **1989**.

[15] G. Menges, F. Knipschild, *Polym. Eng. Sci.* **1975**, *15*, 623.

[16] A. N. Gent, A. G. Thomas, *Rubber Chem. Technol.* **1963**, *36*, 597.

[17] W. L. Ko, *J. Cell. Plast.* **1965**, *1*, 45.

[18] J. M. Lederman, *J. Appl. Polym. Sci.* **1971**, *15*, 693.

[19] C. Redenbach, in *Stereology and Image Analysis. Proc. 10th European Conf. ISS (ECS10)*, Vol. *4*, Bologna, italy **2009**.

[20] Z. Nie, Y. Lin, Q. Tong, *Arch. Metall. Mater.* **2018**, *63*, 1153.

[21] M. Zhang, J. Shang, S. Guo, B. Hur, X. Yue, *Materials* **2021**, *14*, 138.

[22] Q. Sawei, Z. Xinna, H. Qingxian, D. Renjun, J. Yan, H. Yuebo, *Rare Met. Mater. Eng.* **2015**, *44*, 2670.

[23] Y. W. Kwon, R. E. Cooke, C. Park, *Mater. Sci. Eng. A* **2003**, *343*, 63.

[24] L. Vendra, A. Rabiei, *Mater. Sci. Eng. A* **2010**, *527*, 1784.

[25] X. Li, J. Lowengrub, A. Rätz, A. Voigt, *Commun. Math. Sci.* **2009**, *7*, 81.

[26] J. Hötzer, A. Reiter, H. Hierl, P. Steinmetz, M. Selzer, B. Nestler, *J. Comput. Sci.* **2018**, *26*, 1.

[27] A. John, M. John, *Ann. Fac. Eng. Hunedoara* **2016**, *14*, 27.

[28] S. Lloyd, *IEEE Trans. Inf. Theory* **1982**, *28*, 129.

[29] A. G. Khachaturyan, *Theory of Structural Transformations in Solids*, John Wiley and Sons, New York, NY **1983**.

[30] R. Hill, *Proc. R. Soc. London A* **1972**, *326*, 131.

[31] S. Saeb, P. Steinmann, A. Javili, *Appl. Mech. Rev.* **2016**, *68*, 050801.

[32] W. Voigt, *Ann. Phys.* **1889**, *274*, 573.

[33] R. Hill, *Proc. Phys. Soc. Sect. A* **1952**, *65*, 349.

[34] Z. Hashin, S. Shtrikman, *J. Mech. Phys. Solids* **1963**, *11*, 127.

[35] S.-A. Kaoua, D. Dahmoun, A.-E. Belhadj, M. Azzaz, *J. Alloys Compd.* **2009**, *471*, 147.

[36] R. Poli, J. Kennedy, T. Blackwell, *Swarm Intell.* **2007**, *1*, 33.

[37] J. D. Eshelby, *Proc. R. Soc. London, Ser. A* **1957**, *241*, 376.

[38] D. Schneider, F. Schwab, E. Schoof, A. Reiter, C. Herrmann, M. Selzer, T. Böhlke, B. Nestler, *Comput. Mech.* **2017**, *60*, 203.

[39] A. Reuss, *ZAMM - J. Appl. Math. Mech./Z. Angew. Math. Mech.* **1929**, *9*, 49.